AIP | Applied Physics Letters

On-demand hierarchical patterning with electric fields

Qiming Wang, Dominick Robinson, and Xuanhe Zhao

Citation: Applied Physics Letters **104**, 231605 (2014); doi: 10.1063/1.4882416
View online: http://dx.doi.org/10.1063/1.4882416
View Table of Contents: http://scitation.aip.org/content/aip/journal/apl/104/23?ver=pdfcov
Published by the AIP Publishing

On-demand hierarchical patterning with electric fields

Qiming Wang,[1] Dominick Robinson,[1] and Xuanhe Zhao[1,2,a)]
[1]*Department of Mechanical Engineering and Materials Science, Duke University, Durham, North Carolina 27708, USA*
[2]*Soft Active Materials Laboratory, Department of Mechanical Engineering, Massachusetts Institute of Technology, Cambridge, Massachusetts 02139, USA*

(Received 1 April 2014; accepted 18 May 2014; published online 10 June 2014)

We report a method to generate hierarchical topographical patterns on demand under the control of applied voltages. The method is implemented by harnessing the electro-creasing instability in multilayer elastomer films. The critical electric field for electro-creasing instability in a layer of elastomer scales with square root of the elastomer's modulus, while the wavelength of instability pattern scales with the layer's thickness. By rationally designing elastomer films with varied modulus and thickness throughout different layers, we control the formation of surface instability patterns with feature sizes of different scales under prescribed voltages. The method is very versatile, giving various types of hierarchical patterns such as randomly oriented, aligned, and gradient ones. A theoretical model is developed and validated to guide the design of hierarchical patterns. © *2014 AIP Publishing LLC*. [http://dx.doi.org/10.1063/1.4882416]

Nature designs hierarchical structures with feature sizes that range over multiple length scales to achieve extraordinary functions, such as super-hydrophobicity of lotus leaves,[1] strong adhesion of gecko feet,[2] intriguing colors of butterfly wings,[3] and high toughness of animal skeletons.[4] Motivated by these structures and functions, intensive studies have been carried out to design new materials with hierarchical structures.[5–7] Traditional top-down techniques, mostly based on lithography, can be used to fabricate structures with hierarchical features;[8] however, they are generally limited by high-cost and complicated fabrication processes. To overcome these drawbacks, a number of bottom-up strategies based on self-assembly mechanisms have been developed to fabricate hierarchical structures; for instance, capillary-induced assembly of hierarchical pillars or pores,[9] hierarchical instability patterns of thin films,[5,6,10] rationally designed growth of crystal structures,[11] and self-assembly of block copolymers.[12] Among these approaches, using external physical fields (for example, electric fields) to drive the formation of hierarchical structures is particularly compelling, because the pattern-formation process is non-contact, non-destructive, and controlled by external cues.[13] For example, by harnessing electrohydrodynamic instabilities, core-shell structures with hierarchical features have been created on layered thermoplastic polymers.[14] Despite the great promise, hierarchical structures generated by physical fields are mostly static, as the hierarchical structures are fixed at their final states. However, hierarchical structures capable of dynamic control and tunability are highly desirable for various applications such as on-demand super-hydrophobicity,[5,6,15] tunable adhesion,[16] dynamic antifouling,[17] and cell culture.[6,18]

Here, we demonstrate a simple yet effective method that can dynamically generate hierarchical patterns with feature sizes ranging from one to hundreds of micrometers on large-area elastomer surfaces under the control of applied electrical fields. The method is achieved by harnessing the electro-creasing instability in multilayer elastomer films.[19] The critical electric field for inducing electro-creasing instability in a layer of an elastomer scales with square root of the elastomer's modulus, while the wavelength of the instability pattern scales with the layer's thickness.[19–25] By rationally designing multiplayer elastomer films with varied modulus and thickness throughout different layers, we can control the formation of instability patterns with feature sizes of different length scales under prescribed voltages.

The experimental setup for on-demand generation of hierarchical structures under voltages is illustrated in Figs. 1(a) and 1(c). A laminate of two layers of silicone elastomer (Sylgard 184, Dow Corning, USA) was bonded on a rigid polymer substrate (Kapton, DuPont, USA). The bottom Sylgard layer was first spin-coated on Kapton and cured at 65 °C for 12 h, on which the top Sylgard layer was then spin-coated and cured under the same condition. By varying the spinning speed, the thicknesses of the top and bottom silicone layers were obtained as 10–40 μm and 95–250 μm, respectively. The shear moduli of top and bottom elastomers were set to be ~6.7 kPa and ~38.2 kPa, respectively, by tuning the elastomers' cross-linker densities. The shear moduli were measured by uniaxial tensile tests with a Micro-Strain Analyzer (TA Instruments, USA) under a strain rate of $2.5 \times 10^{-4}\,s^{-1}$. The permittivity of the elastomer Sylgard is taken from its data sheet to be $2.65\varepsilon_0$, where $\varepsilon_0 = 8.85 \times 10^{-12}\,F\,m^{-1}$ is the permittivity of vacuum.[26] In addition, the thickness of the substrate Kapton is 125 μm, its shear moduli is 2.5 Gpa and its permittivity is $3.5\varepsilon_0$, taken from the data sheet.[26] Thereafter, the top surface of the elastomer film was immersed in 10 wt. % NaCl solution, which acted as a transparent compliant electrode.[19,23] A direct-current voltage (Mastsusada, Japan) ranging from 0 to 18 kV was applied between the NaCl solution and a metal plate bonded on the substrate with a ramping rate of 10 V/s. The generation of surface patterns was recorded by an optical microscope lens connected with a camera (Nikon, Japan).

a)Author to whom correspondence should be addressed. Electronic mail: zhaox@mit.edu

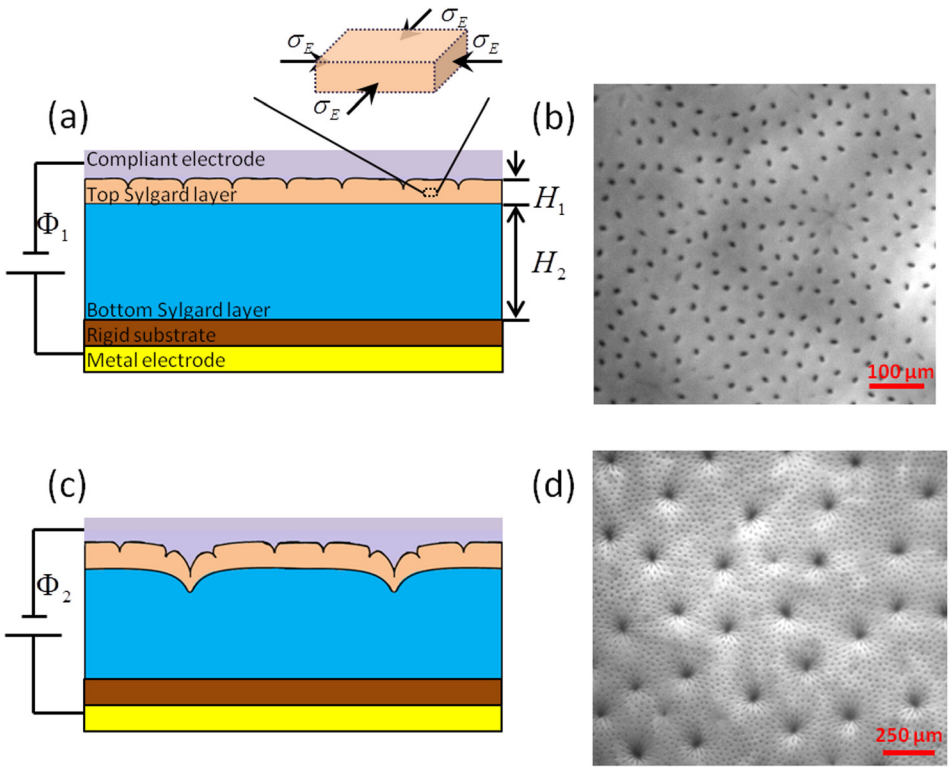

FIG. 1. Cross-section illustrations of the formation of first-order creases on the top Sylgard film (a) and hierarchical creases on the laminate (c). Optical images of the first-order creases (b) and hierarchical creases (d). In (c) and (d), the thicknesses of the top and bottom Sylgard films are ~21 μm and ~200 μm, respectively. The electric fields applied to the laminate are $E_1 = 21\,\text{kV/mm}$ for (c) and $E_1 = 42.4\,\text{kV/mm}$ for (d), respectively.

As shown in Fig. 1(b), when the applied voltage reached a critical value, the initially flat top layer was observed to suddenly fold against itself to form a pattern of creases or dimples. The average wavelength of the crease pattern λ_1 was around 33 μm. Once the voltage was increased to another critical value [Figs. 1(c) and 1(d)], a second-order pattern of creases further developed with wavelength λ_2 around 310 μm, which was evidently larger than the first-order wavelength. In this way, a two-order hierarchical pattern with different wavelengths was generated on the laminate surface. Once the applied voltage was withdrawn, the hierarchical pattern spontaneously disappeared and the surface of the laminate returned to the flat state.

Next, we provide a theoretical model that can guide the design of the hierarchical patterns based on the theory of electro-creasing-to-cratering instability in elastomer films.[19,21,22,25] When an electric field is applied on an elastomer film mechanically constrained on its bottom surface, a biaxial compressive stress σ_E develops along two in-plane directions in the film [see inset of Fig. 1(a)]. Once the compressive stress reaches a critical value, the free surface of the elastomer folds against itself to form a pattern of creases. The critical electric field to induce the crease scales with square root of the shear modulus of the elastomer via[19,21]

$$E_c \approx 1.03\sqrt{\frac{\mu}{\varepsilon}}, \tag{1}$$

where μ and ε are shear modulus and permittivity of the elastomer film, respectively. When the electric field was further ramped up, the creases evolved into a pattern of craters with wavelength λ that scales with the film thickness H as[22]

$$\lambda \approx 1.5H. \tag{2}$$

In the current study, the hierarchical pattern forms in a laminate that consists of a more compliant and thinner elastomer film on top of a stiffer and thicker elastomer film [Figs. 1(a) and 1(c)]. The applied electric fields in the top (E_1) and bottom (E_2) elastomer films can be calculated as

$$E_1 = \frac{\Phi}{H_1 + H_2\varepsilon_2/\varepsilon_1 + H_s\varepsilon_s/\varepsilon_1}, \tag{3a}$$

$$E_2 = \frac{\Phi}{H_2 + H_1\varepsilon_1/\varepsilon_2 + H_s\varepsilon_s/\varepsilon_2}, \tag{3b}$$

where Φ is the applied voltage; μ_1, ε_1, H_1 and μ_2, ε_2, H_2 are the modulus, permittivity, and thickness of the top and bottom elastomer films, respectively; ε_s and H_s are the permittivity and thickness of the rigid substrate.

When the applied voltage is low, the system can be regarded as the top elastomer film constrained on its bottom surface and subjected to an electric field E_1 [Fig. 1(a)]. Once the applied field in the top film reaches a critical value $E_{1c} \approx 1.03\sqrt{\mu_1/\varepsilon_1}$, the creasing instability occurs, giving a pattern of creases with wavelength $\lambda_1 \approx 1.5H_1$. Meanwhile, the deformation in the bottom elastomer film is negligible, since the bottom layer is more rigid than the top layer. Thereafter, when the applied electric field in the bottom elastomer film is increased to a critical value $E_{2c} \approx 1.03\sqrt{\mu_2/\varepsilon_2}$, a second-order pattern of creases form in the bottom film with the top thin film acting as a skin layer. While it is known that the skin layer or surface energy can affect the critical electric field for creasing instability,[20,27] the effect of the skin layer has been observed to be negligible in the current study. Furthermore, following Eq. (2), the wavelength of the second-order pattern is around $\lambda_2 \approx 1.5H_2$.

To validate the above theoretical model for generating hierarchical patterns, a set of experiments were conducted on samples of double-layer Sylgard films with various thickness ratios. As shown in Fig. 2(a), the critical electric fields for

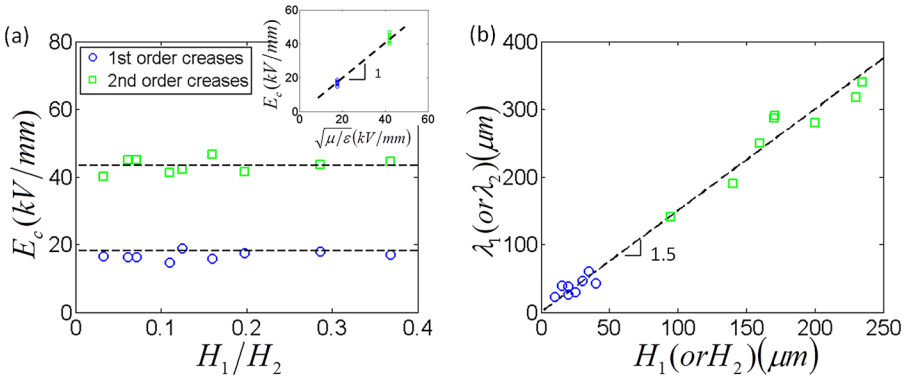

FIG. 2. (a) The critical electric fields for the two-order creases formed on the Sylgard laminates. The inset shows the critical electric fields vary with the shear moduli of two layers of Sylgard films. (b) The wavelengths of two-order creases as functions of the corresponding film thickness.

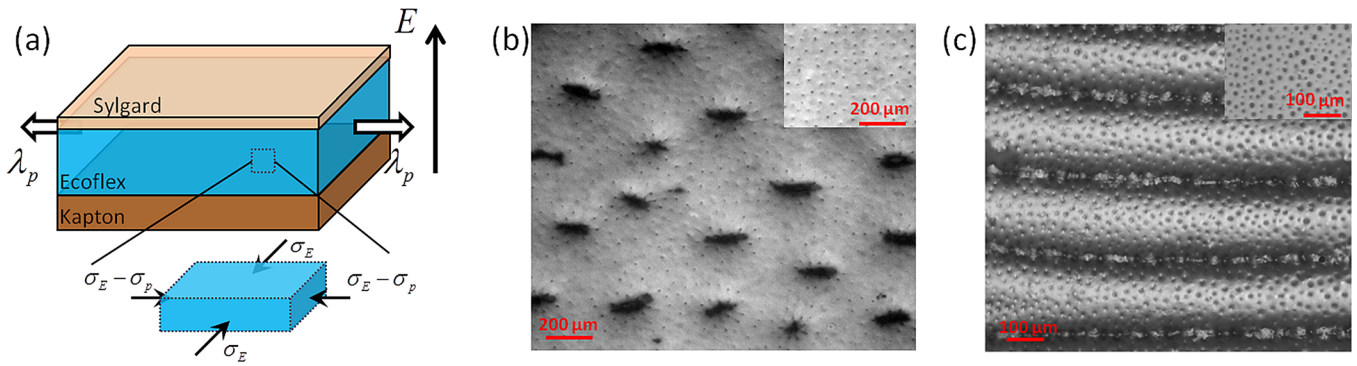

FIG. 3. (a) Schematic to show the stress state of the pre-stretched elastomer under an electric field E. The electric-field-induced compressive stress σ_E is offset by the tensile stress from pre-stretch σ_p. Examples of aligned hierarchical patterns: (b) randomly distributed first-order creases coexist with aligned second-order creases ($\lambda_p = 2$), and (c) randomly distributed first-order creases coexist with aligned second-order lines ($\lambda_p = 5$). Insets in (b) and (c) show the randomly distributed first-order creases only. The thickness of the bottom elastomer film in (b) is 358 μm before pre-stretch, and reduced to 253 μm under pre-stretch $\lambda_p = 2$. The thickness of the bottom elastomer film in (c) is 452 μm before pre-stretch and reduced to 203 μm under pre-stretch $\lambda_p = 5$.

inducing two orders of patterns indeed fall on two levels for various ratios of film thicknesses. Furthermore, the critical electric fields approximately match the theoretical prediction, i.e., $E_{1c} \approx \sqrt{\mu_1/\varepsilon_1}$ and $E_{2c} \approx \sqrt{\mu_2/\varepsilon_2}$ [inset of Fig. 2(a)]. In addition, the measured wavelengths of the two orders of patterns are plotted as functions of the thicknesses of the two layers in Fig. 2(b). It can be seen that the slope of the data points in Fig. 2(b) is around 1.5, which also matches the theoretical prediction, i.e., $\lambda_1 \approx 1.5H_1$ and $\lambda_2 \approx 1.5H_2$.

Next, we demonstrate the versatility of the method to generate different types of hierarchical patterns. For example, aligned hierarchical patterns can be readily achieved by pre-deforming the elastomer films prior to attaching them on the substrate [Fig. 3(a)]. A silicone elastomer Ecoflex (Smooth-On, USA) was chosen as the bottom elastomer film due to its high stretchability. The modulus of the bottom Ecoflex film was 10.4 kPa, and the thickness was varied from 120 to 250 μm.[21,22] The permittivity of the elastomer Ecoflex is taken from its data sheet to be $2.5\varepsilon_0$, where $\varepsilon_0 = 8.85 \times 10^{-12}\,\mathrm{Fm}^{-1}$ is the permittivity of vacuum.[26] The Ecoflex film was first stretched uniaxially by a factor of λ_p, and then adhered to a rigid Kapton film to preserve the pre-stretch. On the pre-stretched Ecoflex film, another thin film of Ecoflex was casted with thickness of 15–30 μm and modulus of 5.4 kPa. In this way, the first-order pattern of creases generated in the top film was still randomly oriented. However, since the pre-stretch offset the electric-field-induced compressive stress in the bottom film, the second-order creases formed in the bottom film tend to align along the pre-stretched direction[22] [Fig. 3(b)]. Furthermore, if the pre-stretch ratio is high, e.g., 5 in Fig. 3(c), the aligned creases can connect with one other into a pattern of aligned lines in the bottom film.[22]

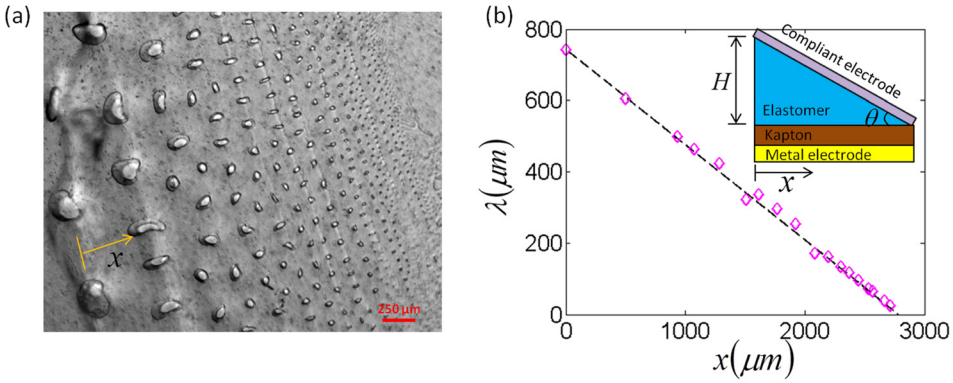

FIG. 4. (a) A pattern of creases and craters formed on a Sylgard film with a gradient thickness from 0 μm to 205 μm. (b) The measured wavelength of the craters formed on the Sylgard film as a function of the distance from the thicker edge of the film compared with the prediction of Eq. (4). The dashed line denotes the theoretical prediction from Eq. (4). The inset of (b) shows the schematic illustration of the experiment setup.

As another example, we demonstrate the dynamic generation of surface patterns with continuously varied feature sizes under the control of electric fields. A Sylgard film with thickness of 250 μm was first spin-coated on a Kapton substrate. Following the curing, the Sylgard film was tapered by cutting it with a titled knife of angle θ against the substrate surface. As a result, we obtained a Sylgard film with a gradient thickness, from 205 μm to $\sim$0 μm [inset of Fig. 4(b)]. A ramping electric field is applied through the Sylgard film. The creasing instability first occurs on the surface of the thinner region of the film and gradually spreads to the thicker region, as shown in Fig. 4(a). Based on Eq. (1), the wavelength of the pattern is thus continuously varied as

$$\lambda \approx 1.5(H - x\tan\theta), \tag{4}$$

where x is the distance from the thicker edge of the film. In Fig. 4(b), we plot the experimentally measured wavelength of the pattern as a function of x. It can be seen that the experimental data match consistently with the prediction of Eq. (4).

In summary, we report a simple yet effective method to generate hierarchical patterns on elastomer films under the control of applied voltages. By tuning the thicknesses, moduli and pre-deformation of the multilayer elastomer films, we demonstrate that various hierarchical patterns with different feature sizes, alignments and gradients can be dynamically generated with this versatile method. We further develop a theoretical model to guide the design of the hierarchical patterns, capable of predicting the critical electric fields and wavelengths of the patterns. These new dynamic hierarchical patterns are expected to find useful applications in diverse fields such on-demand super-hydrophobicity,[15] tunable adhesion and wetting,[16] dynamic antifouling,[17] and controlled cell alignment.[18]

The work was supported by NSF CAREER Award No. (CMMI-1253495), NSF Grant No. (CMMI-1200515), NSF Triangle MRSEC No. (DMR-1121107), and NIH Grant No. (UH2 TR000505).

[1]C. Neinhuis and W. Barthlott, Ann. Bot. **79**(6), 667 (1997).
[2]K. Autumn, Y. A. Liang, S. T. Hsieh, W. Zesch, W. Pang Chan, T. W. Kenny, R. Fearing, and R. J. Full, Nature **405**(6787), 681 (2000).
[3]P. Vukusic and J. R. Sambles, Nature **424**(6950), 852 (2003).
[4]J. Aizenberg, J. C. Weaver, M. S. Thanawala, V. C. Sundar, D. E. Morse, and P. Fratzl, Science **309**(5732), 275 (2005).
[5]J. Zang, S. Ryu, N. Pugno, Q. Wang, Q. Tu, M. J. Buehler, and X. Zhao, Nature Mater. **12**(4), 321 (2013).
[6]C. Cao, H. F. Chan, J. Zang, K. W. Leong, and X. Zhao, Adv. Mater. **26**(11), 1763 (2014).
[7]A. Honglawan and S. Yang, Soft Matter **8**(47), 11897 (2012); A. Honglawan, D. A. Beller, M. Cavallaro, R. D. Kamien, K. J. Stebe, and S. Yang, Proc. Natl. Acad. Sci. U. S. A. **110**(1), 34 (2013).
[8]H. Lee, B. P. Lee, and P. B. Messersmith, Nature **448**(7151), 338 (2007); A. K. Geim, S. V. Dubonos, I. V. Grigorieva, K. S. Novoselov, A. A. Zhukov, and S. Yu. Shapoval, Nature Mater. **2**(7), 461 (2003); P. Yang, T. Deng, D. Zhao, P. Feng, D. Pine, B. F. Chmelka, G. M. Whitesides, and G. D. Stucky, Science **282**(5397), 2244 (1998); Z. Nie and E. Kumacheva, Nature Mater. **7**(4), 277 (2008); Y. Xia and G. M. Whitesides, Annu. Rev. Mater. Sci. **28**(1), 153 (1998).
[9]B. Pokroy, S. H. Kang, L. Mahadevan, and J. Aizenberg, Science **323**(5911), 237 (2009); X. Zhu, G. Wu, R. Dong, C.-M. Chen, and S. Yang, Soft Matter **8**(31), 8088 (2012).
[10]Z. Zhang, T. Zhang, Y. W. Zhang, K.-S. Kim, and H. Gao, Langmuir **28**(5), 2753 (2012); Q. Wang and X. Zhao, J. Appl. Mech. **81**(5), 051004 (2013).
[11]W. L. Noorduin, A. Grinthal, L. Mahadevan, and J. Aizenberg, Science **340**(6134), 832 (2013).
[12]W. A. Lopes and H. M. Jaeger, Nature **414**(6865), 735 (2001).
[13]Z. Yu, W. Yuan, P. Brochu, B. Chen, Z. Liu, and Q. Pei, Appl. Phys. Lett. **95**(19), 192904 (2009); I. A. Anderson, T. A. Gisby, T. G. McKay, B. M. O'Brien, and E. P. Calius, J. Appl. Phys. **112**(4), 041101 (2012).
[14]M. D. Morariu, N. E. Voicu, E. Schäffer, Z. Lin, T. P. Russell, and U. Steiner, Nature Mater. **2**(1), 48 (2003); P. Goldberg-Oppenheimer, S. Mahajan, and U. Steiner, Adv. Mater. **24**(23), OP175 (2012); M. D. Dickey, S. Gupta, K. A. Leach, E. Collister, C. G. Willson, and T. P. Russell, Langmuir **22**(9), 4315 (2006).
[15]T. Sun, G. Wang, L. Feng, B. Liu, Y. Ma, L. Jiang, and D. Zhu, Angew. Chem., Int. Ed. **43**(3), 357 (2004).
[16]H. Gao and H. Yao, Proc. Natl. Acad. Sci. U. S. A. **101**(21), 7851 (2004); E. P. Chan, E. J. Smith, R. C. Hayward, and A. J. Crosby, Adv. Mater. **20**(4), 711 (2008).
[17]P. Shivapooja, Q. Wang, B. Orihuela, D. Rittschof, G. P. López, and X. Zhao, Adv. Mater. **25**(10), 1430 (2013); V. Levering, Q. Wang, P. Shivapooja, X. Zhao, and G. P. López, "Soft robotic concepts in catheter design: An on-demand fouling-release urinary catheter," Adv. Healthcare Mater. (published online 2014).
[18]R. G. Thakar, F. Ho, N. F. Huang, D. Liepmann, and S. Li, Biochem. Biophys. Res. Commun. **307**(4), 883 (2003); K. Kurpinski, J. Chu, C. Hashi, and S. Li, Proc. Natl. Acad. Sci. **103**(44), 16095 (2006).
[19]Q. Wang, L. Zhang, and X. Zhao, Phys. Rev. Lett. **106**(11), 118301 (2011).
[20]Q. Wang and X. Zhao, Phys. Rev. E **88**(4), 042403 (2013).
[21]Q. Wang, M. Tahir, L. Zhang, and X. Zhao, Soft Matter **7**(14), 6583 (2011).
[22]Q. Wang, M. Tahir, J. Zang, and X. Zhao, Adv. Mater. **24**(15), 1947 (2012).
[23]Q. Wang, Z. Suo, and X. Zhao, Nat. Commun. **3**, 1157 (2012).
[24]Q. Wang, X. Niu, Q. Pei, M. D. Dickey, and X. Zhao, Appl. Phys. Lett. **101**(14), 141911 (2012).
[25]X. Zhao and Q. Wang, Appl. Phys. Rev. **1**, 021304 (2014).
[26]Date sheets of Sylgard 184, Ecoflex 0010 and Kapton.
[27]D. Chen, S. Cai, Z. Suo, and R. C. Hayward, Phys. Rev. Lett. **109**(3), 038001 (2012).